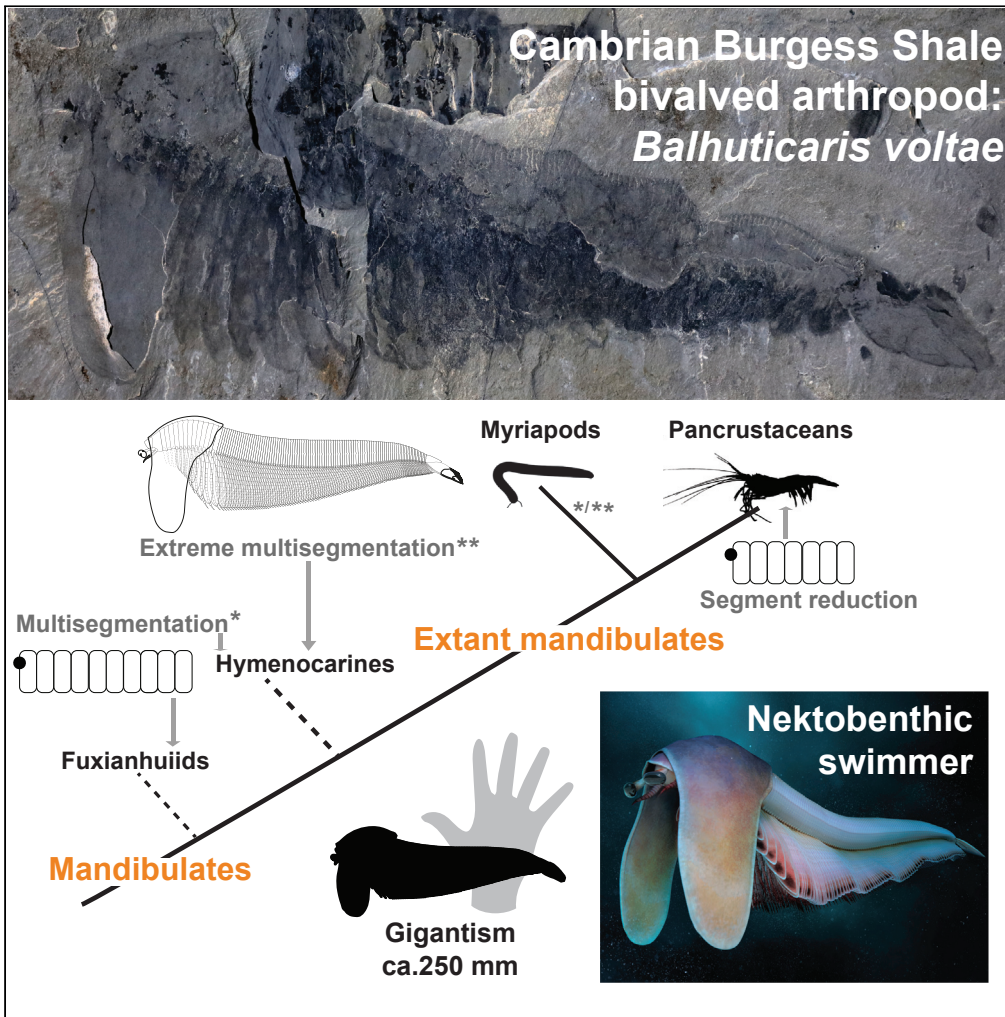


Article

Extreme multisegmentation in a giant bivalved arthropod from the Cambrian Burgess Shale



Alejandro Izquierdo-López, Jean-Bernard Caron

ai.lopez@mail.utoronto.ca

Highlights
Balhuticaris voltae; a bivalved arthropod from the Cambrian Burgess Shale

It is the largest bivalved arthropod and one of the largest Cambrian arthropods

It was an agile nektobenthic swimmer with an extremely multisegmented body

This species increases the ecological and functional disparity of bivalved arthropods

Izquierdo-López & Caron, iScience 25, 104675 July 15, 2022 Crown Copyright © 2022 <https://doi.org/10.1016/j.isci.2022.104675>

Article

Extreme multisegmentation in a giant bivalved arthropod from the Cambrian Burgess Shale

Alejandro Izquierdo-López^{1,2,4,*} and Jean-Bernard Caron^{1,2,3}

SUMMARY

The origin of mandibulate arthropods can be traced back to the Cambrian period to several carapace-bearing arthropod groups, but their morphological diversity is still not well characterized. Here, we describe *Balhuticaris voltae*, a bivalved arthropod from the 506-million-year-old Burgess Shale (Marble Canyon, British Columbia, Canada). This species has an extremely elongated and multisegmented body bearing ca. 110 pairs of homonomous biramous limbs, the highest number among Cambrian arthropods, and, at 245 mm, it represents one of the largest Cambrian arthropods known. Its unusual carapace resembles an arch; it covers only the frontalmost section of the body but extends ventrally beyond the legs. *Balhuticaris* had a complex sensory system and was probably an active swimmer thanks to its powerful paddle-shaped exopods and a long and flexible body. *Balhuticaris* increases the ecological and functional diversity of bivalved arthropods and suggests that cases of gigantism occurred in more arthropod groups than previously recognized.

INTRODUCTION

Cambrian bivalved arthropods are a group of arthropods characterized by their cephalothoracic bivalved carapaces. Many bivalved arthropods are known only from isolated carapaces, but fossils with soft tissue preservation are revealing an increasingly complex group, mostly comprising the stem-group euarthropod Isoxyidae (Aria and Caron, 2015) and the Hymenocarina. With 30–40 known species, hymenocarines are the more diverse of both groups, but their position in early arthropod evolution has been widely debated. Originally early euarthropods (Legg et al., 2012; Legg and Caron, 2014), the recent discovery of mandibles in multiple species (Aria and Caron, 2017; Vannier et al., 2018; Zhai et al., 2019), rather indicates an affinity with mandibulates (myriapods, crustaceans, and insects), most probably as early mandibulates (Aria and Caron, 2017) or stem-pancrustaceans (Vannier et al., 2018; Zhai et al., 2019). In most hymenocarines, though, the carapace obscures the cephalon, contributing to a lack of information regarding the cephalic conformation of most species (Izquierdo-López and Caron, 2021). Furthermore, certain traits are often not preserved in detail (e.g., legs, Izquierdo-López and Caron, 2019), which has similarly impacted our understanding of their phylogenetic placement. Open questions for this group include their monophyly (Aria, 2020), their exact position with respect to the mandibulate crown group (Aria, 2022), and their relation to other Cambrian arthropod groups (e.g., fuxianhuiids, Aria et al., 2021). Regardless, hymenocarines continue to represent one of the best candidates for stem- or early mandibulate groups, and their increasingly richer fossil record allows us to start tackling questions about the ancestral body plan of the earliest mandibulates, including thoracic segmentation and tagmatization.

The hymenocarine fossil record also showcases high ecological diversity. Feeding strategies among hymenocarines were diverse, and probably included deposit feeding (Legg and Caron, 2014), scavenging (Vannier et al., 2018), predation (Yang et al., 2016), and suspension feeding (Legg et al., 2012). It has also been suggested that some species could have switched between feeding strategies (Jin et al., 2021), which better reflects the behavior of many extant crustaceans (Caine, 1974; Macneil et al., 1997). Hymenocarines also present a wide array of carapace shapes, which could suggest it was a functionally complex structure (Olesen, 2013), and hold some of the first records of several behaviors observed in extant mandibulates, such as chain-like associations (Hou et al., 2009), synchronized moulting (Haug et al., 2013), brood care (Caron and Vannier, 2016), and upside-down swimming (Briggs, 1981; Izquierdo-López and Caron, 2019).

Here, we describe a Cambrian bivalved arthropod, a potential mandibulate hymenocarine, based on 11 specimens from the Marble Canyon area of the Burgess Shale (Canada). This species is the largest bivalved arthropod

¹Department of Ecology and Evolutionary Biology, University of Toronto, 25 Willcocks Street, Toronto, ON M5S 3B2, Canada

²Department of Natural History, Palaeobiology, Royal Ontario Museum, 100 Queen's Park, Toronto, ON M5S 2C6, Canada

³Department of Earth Sciences, University of Toronto, 22 Russell Street, Toronto, ON M5S 3B1, Canada

⁴Lead contact

*Correspondence:

ai.lopez@mail.utoronto.ca

<https://doi.org/10.1016/j.isci.2022.104675>



to date, at almost double the size of the previous record-holder (*Nereocaris exilis*, Legg et al., 2012). It has the highest number of segments of any Cambrian arthropod and also exhibits a distinct segmental differentiation, unlike other hymenocarine post-cephalic tagmatization patterns. Furthermore, it also bears a uniquely shaped carapace that covers only the frontalmost section of the trunk, and a pair of laterally bilobed eyes, highly unusual in the early arthropod fossil record that highlight the functional and ecological diversity of this group.

RESULTS

Preservation

All specimens (n = 11) are preserved as two-dimensional compressed carbonaceous and aluminosilicate films. The holotype and three additional specimens are complete or nearly complete (Figures 1B, 5A, S1A, S1B, and S2C), although some specimens show evidence of pre-burial decay and disarticulation (Figures 1D, S1C, and S2A). The height of the trunk appears sometimes uneven, likewise indicating compression artifacts, and, potentially, weak sclerotization of the segments (Figures 1B, 2B, S2A). Compression folds suggest that the carapace was also weakly mineralized (Figure 1D).

Systematic paleontology

Phylum

Arthropoda von Siebold, 1848 (Hegna et al., 2013).

Subphylum

Mandibulata Snodgrass (1938) (Snodgrass, 1938).

Genus

Balhuticaris voltae gen. et sp. nov.

Etymology

Balhuticaris, from *Balhūt* (Bahamut), a gigantic sea monster from several Persian cosmographies, and the Latin *caris*, crab. Species name *voltae* from the Catalan *volta*, meaning vault or arch-like structure, referring to the shape of the carapace in frontal view.

Holotype

ROMIP66238 (Figures 1A–1C, 2B, and 5A).

Referred material

Additional specimens ROMIP66235–ROMIP66244 (Figures 1, 2, S1, and S2; Supplemental information).

Diagnosis for genus and species

Bivalved arthropod with a carapace sub-equal to or greater in height than length, covering the frontalmost section of the body and extending anteroventrally beyond the level of the longest cephalothoracic legs; stalked eyes laterally bilobate. Total number of post-cephalic segments ca. 110:10–12 thoracic segments and ca. 100 post-thoracic segments. Each thoracic segment is three times longer than a post-thoracic segment. Caudal rami tripartite, with pseudo-segments bearing elongated setae distally.

Description

Specimens with their full body preserved measured 171.8 mm (Figures 1A, 1B, and 5A), 198.0 mm (Figure S2C), and 244.7 mm (Figures S1A and S1B), to a total mean length of ca. 205 mm.

In lateral view, the carapace covers the cephalon and the frontalmost part of the trunk. The carapace extends ventrally from both sides into two valves fused dorsally, forming a dome-like structure (Figure 1E). The valves in the frontal section of the carapace have a straight margin. They extend ventrally beyond the level of the longest cephalothoracic legs and terminate in a convex ventral margin. The posterior edge is straight, but becomes concave closer to the dorsal side of the carapace, transitioning into the posterior section of the carapace. In the posterior section of the carapace, the carapace valves extend ventrally only up to the ventral side of the trunk. The valves extend further posteriorly and have a concave to strongly postplete posterior margin (Figures 1A, 1B, and 1E).

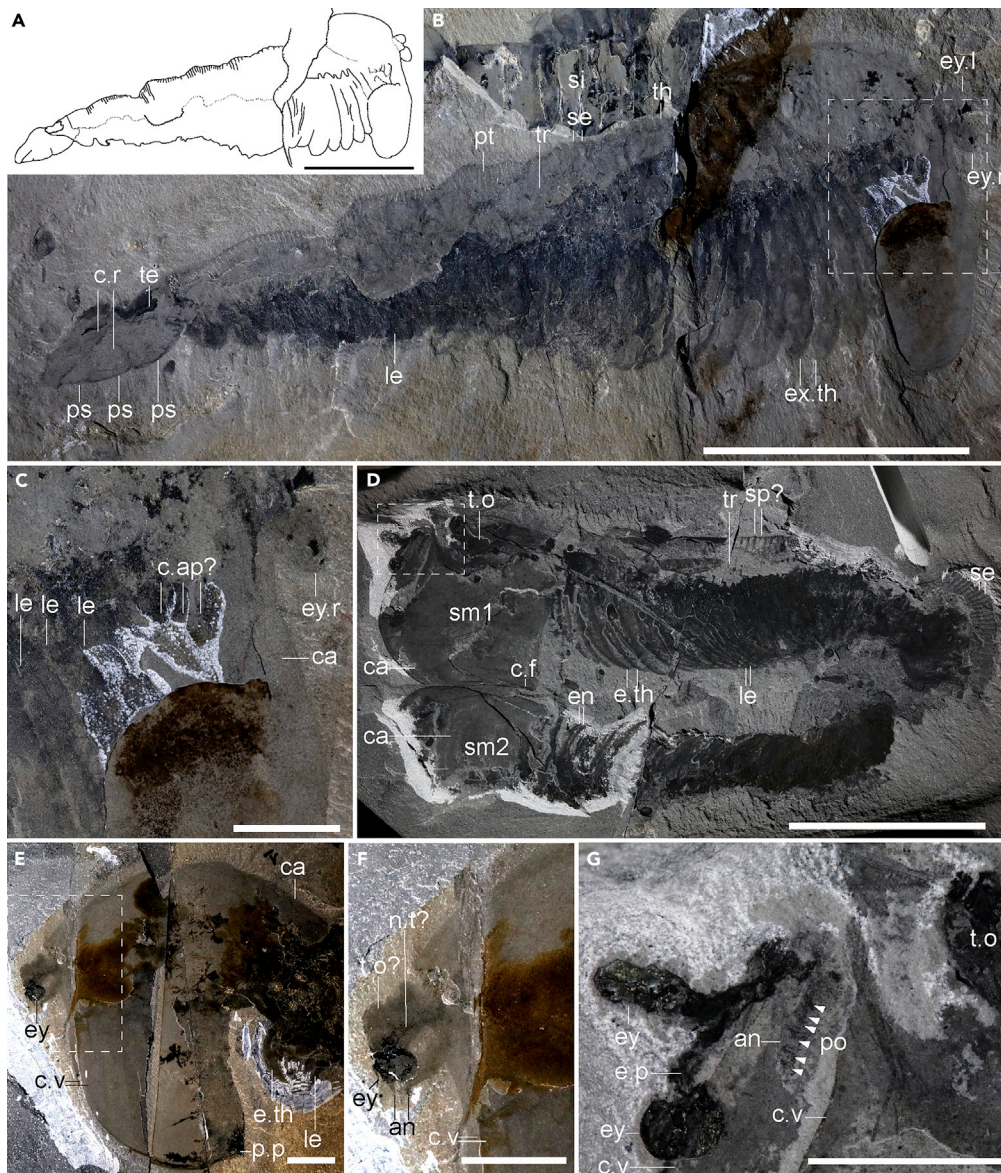


Figure 1. Overall habitus and head of *Balhutaris voltae*

(A–C) Holotype (ROMIP66238) shown through a camera lucida drawing (A), a full lateral view of the body (B) and a close-up of the cephalic area (C) after manually removing the carapace, showing several pairs of cephalic appendages. (D) Two specimens partly preserved in lateral view (ROMIP66243), facing each other, and close-up of the cephalic area of the upper specimen (G), showing the bilobate eyes, ocular tergite and the antenna. (E) Cephalic region (ROMIP66236), showing the Morpho-type B carapace, and close-up of the cephalic area (F). Abbreviations: an, antenna; ca, carapace; c.ap, cephalic appendage; c.f., compression fold; c.r, caudal rami; c.v, carapace valves; ey.l, left eye; ey.r, right eye; en, endopod; e.th, endopod thorax; ex.th, exopod thorax; le, leg; n.t, nervous tissue; po, podomere; p.p, posterior process; ps, pseudo-segment; pt, post-thorax; se, segments; si, *Sidneyia inexpectans*; sm, specimen; sp, spine; te, telson; th, thorax; t.o, tergite of the ocular segment; tr, trunk. Scales: (A, B, D) 50 mm; (C, E–G) 10 mm. See also [Figures S1](#) and [S2](#).

Two morphotypes may be present based on the relative widths of the carapace and the shape of the posteroventral margin. In morphotype A, the carapace covers ca. 25% of the total body length dorsally, while the frontal section covers only 10% of the total body length ([Figures 1A, 1B, 2E, 3A, 5A, S1A, S1B](#)). In morphotype B, the frontal section of the carapace is longer, and the posterior section of the carapace also extends further posteriorly, covering a higher number of segments ([Figures 1D, 1E, 3A.1, S1C, and S2B](#)). In this

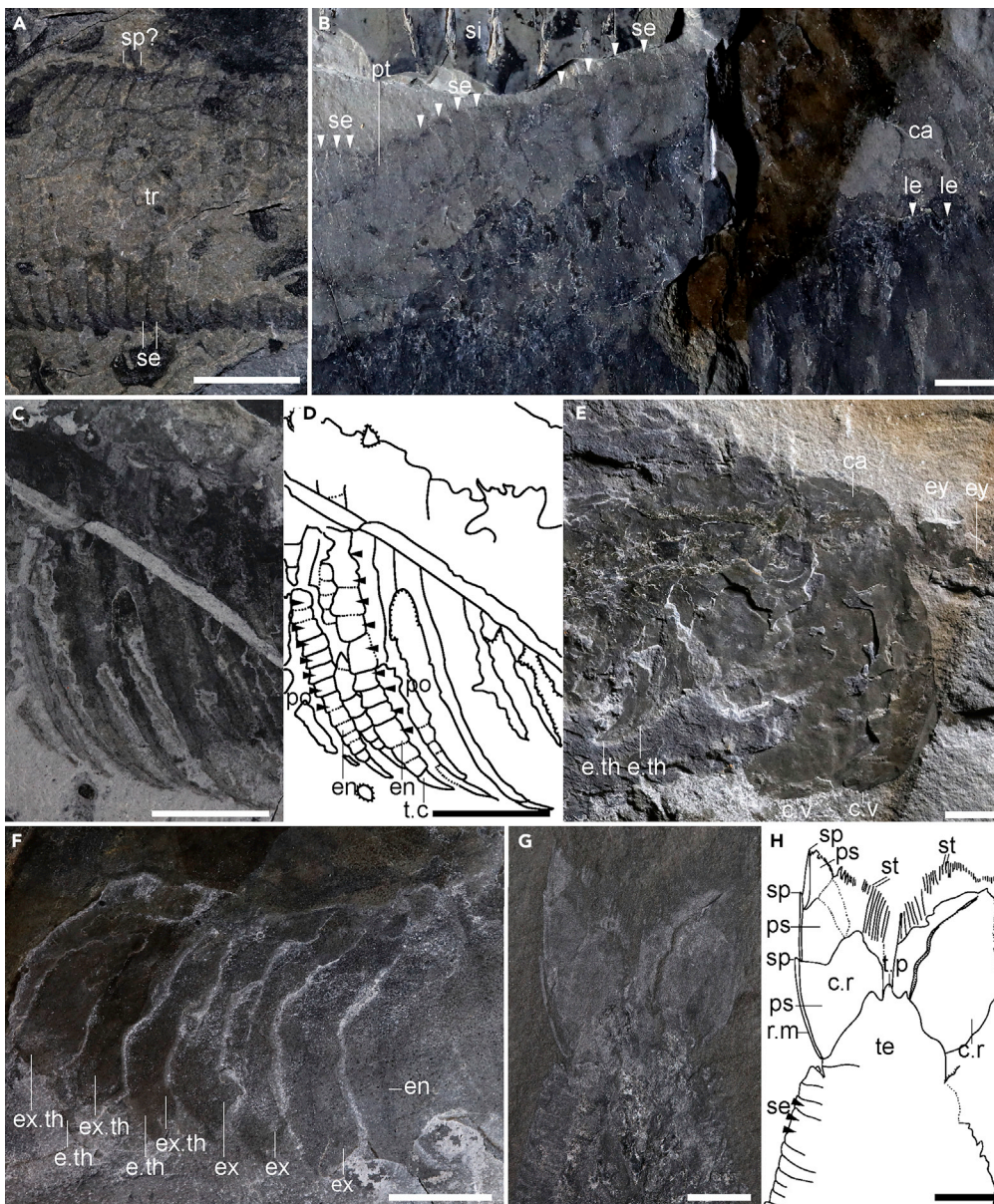


Figure 2. Trunk, legs, and telson of *Balhuticaris voltae*

(A) Trunk (ROMIP66244) showing segments expanding laterally into spines.
 (B) Close-up of the trunk segments (ROMIP66238) in which the thoracic segments are longer than in the post-thorax.
 (C) Endopods (ROMIP66243) and their interpretation through camera lucida (D), highlighting podomeres.
 (E) Frontal section (ROMIP66242) in which the thoracic endopods are thicker than the post-thoracic endopods but become shorter anteriorly.
 (F) Legs (ROMIP66239), showing exopods.
 (G) Close-up of the telson and caudal rami (ROMIP66241) and camera lucida drawing (H). Abbreviations: po, podomere; ps, pseudo-segment; r.m, reinforced margin; st, setae; t.c, terminal claw (podomere); t.p, telson process. Other abbreviations as in Figure 1. Scales: A-H) 10 mm. See also Figures S1–S3.

morphotype, the carapace also bears a blunt process on the posteroventral margin of the frontal section (Figures 1E and S2B). Morphotypes may indicate sexual dimorphism, regional variations, or may represent different variations in a broader range of carapace shapes. The limited number of specimens precludes further discussion on this topic. Because both morphotypes were retrieved from similar stratigraphic horizons, we interpret them as members of the same species.

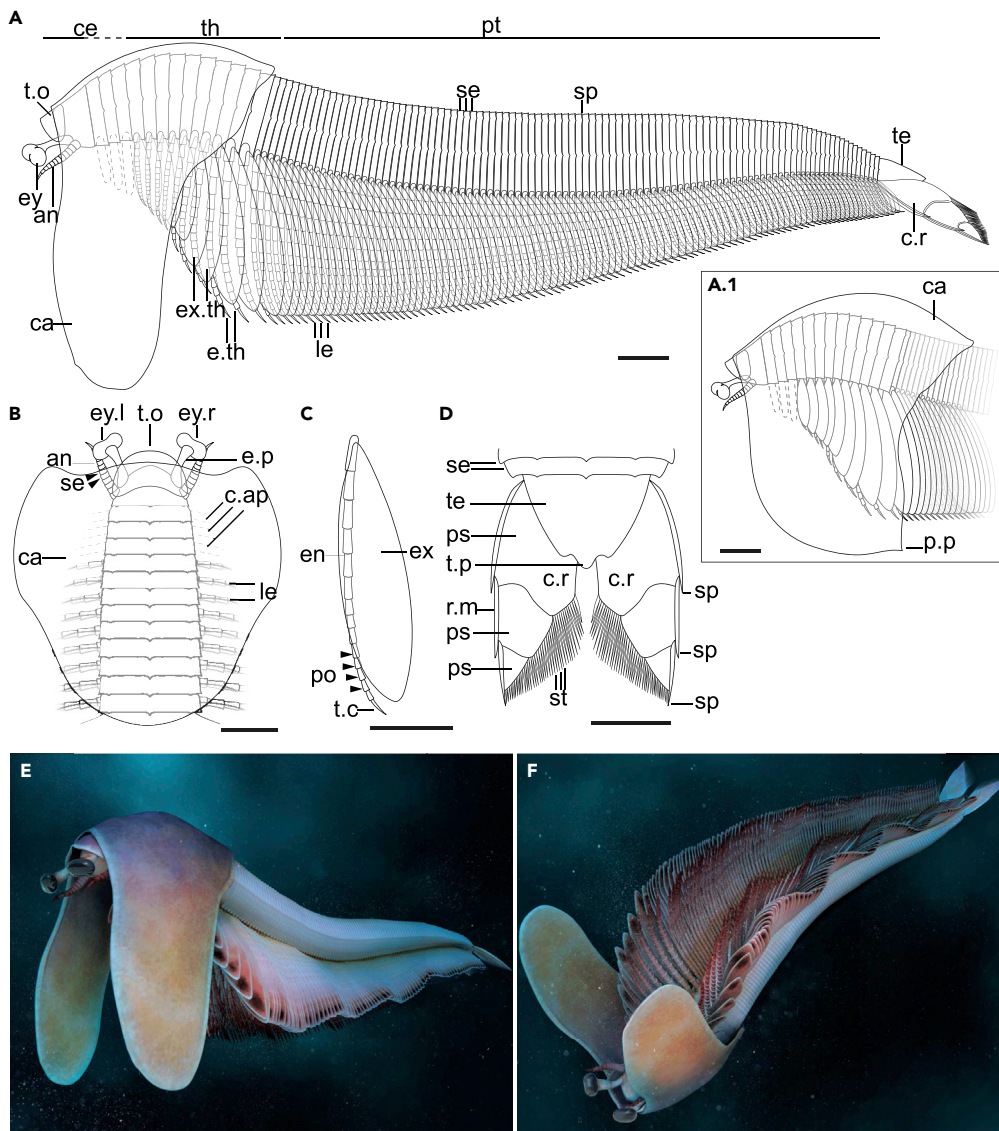


Figure 3. Reconstruction of *Balhuticaris voltae*

Full body in lateral view (A), close-up of (A) with the morphotype B type of carapace (A.1), close-up of the cephalic area in dorsal view (B), leg (C), and close-up of the telson and caudal rami in dorsal view (D).

Artistic reconstruction (E) and alternative artistic reconstruction swimming inverted (F). All reconstructions courtesy of Hugo Salais. Abbreviations: ce, cephalon (head). Other abbreviations as in Figures 1 and 2. Scales: A-D) 10 mm.

The ocular segment extends slightly beyond the frontal side of the carapace, bearing a pair of pedunculate eyes (Figures 1C–1F). Eyes are laterally bilobate (Figures 1F and 1G). Eye peduncles are probably inserted at the base of the ocular segment and are longer than the segment itself (Figure 1F). Dark tissue running through the peduncle may represent neural tissue (Figures 1F and 1G). A large elongated crescent-shaped tergite covers at least the ocular segment, probably overlapping with the carapace (Figures 1D–1G, S2E and S2F). The tergite resembles the carapace in its level of sclerotization but is not visible in all specimens, potentially displaced or hidden by the carapace (ROMIP66240).

A pair of cephalic appendages interpreted as deutocerebral antennae (i.e., antennulae) originates posteriorly to the base of the eye peduncles. These appendages are uniramous, thick, tapering in width frontally, and slightly longer than the eye peduncles (Figures 1D–1G). Podomeres are visible in one antenna, partly preserved (Figure 1G). Considering that the length of the podomeres may remain constant, their

number would be 11–12. The partial removal of the carapace in other specimens reveals 5–6 short, poorly preserved limbs posterior to the antennae (Figure 1C). The shortest first three limbs could be part of the head, but their morphology is uncertain. The following limbs appear consistent in shape with the more posterior biramous limbs of the trunk and most probably belong to that body section.

The trunk is multisegmented, with ca. 110 segments, discernible as tergo-pleural rings (Figures 1B and 2A). These are generally homonomous but decrease in width and height posteriorly. The 10–12 thoracic segments are the longest (thorax), with a mean length of 3.2 mm (Figure 2B). Posterior segments are significantly shorter (post-thorax), and decrease further in length, with a mean length of 1.12 mm (Supplemental information). Segments appear round to slightly pentagonal in cross-section (Figures S2C and S2D). In lateral view, each segment expands in width posteriorly and may bear one postero-dorsally small blunt spine (Figures 1D and S2D) and two laterally small blunt spines (Figures 2A and 3B), although these could also be interpreted as the shape of the anterior segment, overlapping the following segment. A faint trace across the trunk is interpreted as fossilized gut content (Figure S2D).

All trunk segments bear a pair of biramous legs (Figure 1B). The first 10–12 pairs correspond to the thoracic section with enlarged segments, decrease in size anteriorly, but bear endopods slightly thicker than the limbs from the post-thoracic region (Figures 1B, 1C, 2C, 2D, 2F, and S2F). Post-thoracic limbs become gradually smaller toward the posterior end of the body. Endopods in both sections of the trunk are thin and elongated, slightly recurved, subdivided into ca. 14–15 podomeres (Figures 2C and 2D). All podomeres have a similar shape, with each podomere expanding distally in width, but overall decreasing in size in relation to the more proximal podomeres. The distalmost podomere is highly elongated in comparison (Figures 2C and 2D). Exopods are ellipsoid to circular, slightly shorter than the endopods, originating close to the base of the limbs, but their exact point of attachment is unknown (Figures 1B, 1C, 2F, and S2F).

The telson is narrow, dorsoventrally flat, and equivalent in length to ca. 15% of the total length of the body (Figures 1B, 2G, and 2H). In dorsal view, its outline is semicircular, probably terminating in three small blunt processes (Figures 2G, 2H, and S3K). The telson bears two paddle-shaped caudal rami. The outer margin of each ramus is convex, with a reinforced margin, while the inner margin is initially straight, but bends posteriorly until converging with the outer margin, and bears multiple long setae. Each ramus is tripartite; subdivided into three pseudo-segments, which become smaller posteriorly, with the posteriormost one being almost triangular. The outer margin of each pseudo-segment extends posteriorly into a small spine (Figures 2G, 2H, and S3K).

Phylogenetic affinities

Balhtucaris is recovered within Hymenocarina (Figures 4A and S4), as a stem-Pancrustacean group, although with low support (Figure S4). Given that mandibulates appear monophyletic with higher support, we prefer to consider hymenocarines as early mandibulates, following previous analyses (Aria, 2020). Whether hymenocarines are retrieved as monophyletic or not depends on the dataset analyzed. In a hymenocarine-centric dataset (Figure 4A), they are recovered as paraphyletic, including fuxianhuiids (Aria, 2020; Aria et al., 2021), but in an all-euarthropod dataset, they are recovered as monophyletic (Izquierdo-López and Caron, 2021), but with low support (Figure S4). Both analyses retrieve the different hymenocarine families and orders (see Zeng et al., 2020 for a general overview): perspicaridids and canadaspidids (Canadaspida) (Orlov, 1960; Zeng et al., 2020), waptiids (Walcott, 1912), clypecaridids (Hou, 1999), protocaridids (Aria and Caron, 2017; Miller, 1889), and “odaraiids” (e.g., *Odaraiia*, *Nereocaris*, *Pakucaris*, and *Fibulacaris*) (Izquierdo-López and Caron, 2019, 2021). *Balhtucaris* is retrieved within “odaraiids” in all datasets, but the monophyly of this group varies across the presented phylogenies. Given the generally low support of some of these groups, a morphospace was created to visualize phenetic similarities within hymenocarines. The morphospace (Figure 4B) separates the main hymenocarines groups and *Balhtucaris* appears within a cluster of other “odaraiids”. The occupation of the morphospace by hymenocarines is characterized by a high variation of certain morphological features (e.g., degree of development of the antennae), while other traits remain constrained (e.g., paddle-shaped exopods), leading to widely separated morphotypes (Aria, 2020). The first component of the analysis (Figure 4B) portrays this tendency, aligning hymenocarines together but widely separating groups such as protocaridids and “odaraiids”. Based on the present evidence, we regard *Balhtucaris* as a potential early mandibulate hymenocarine. However, the affinity of this and other closely related taxa may change in the light of new information regarding their cephalic conformation and the morphology of the legs.

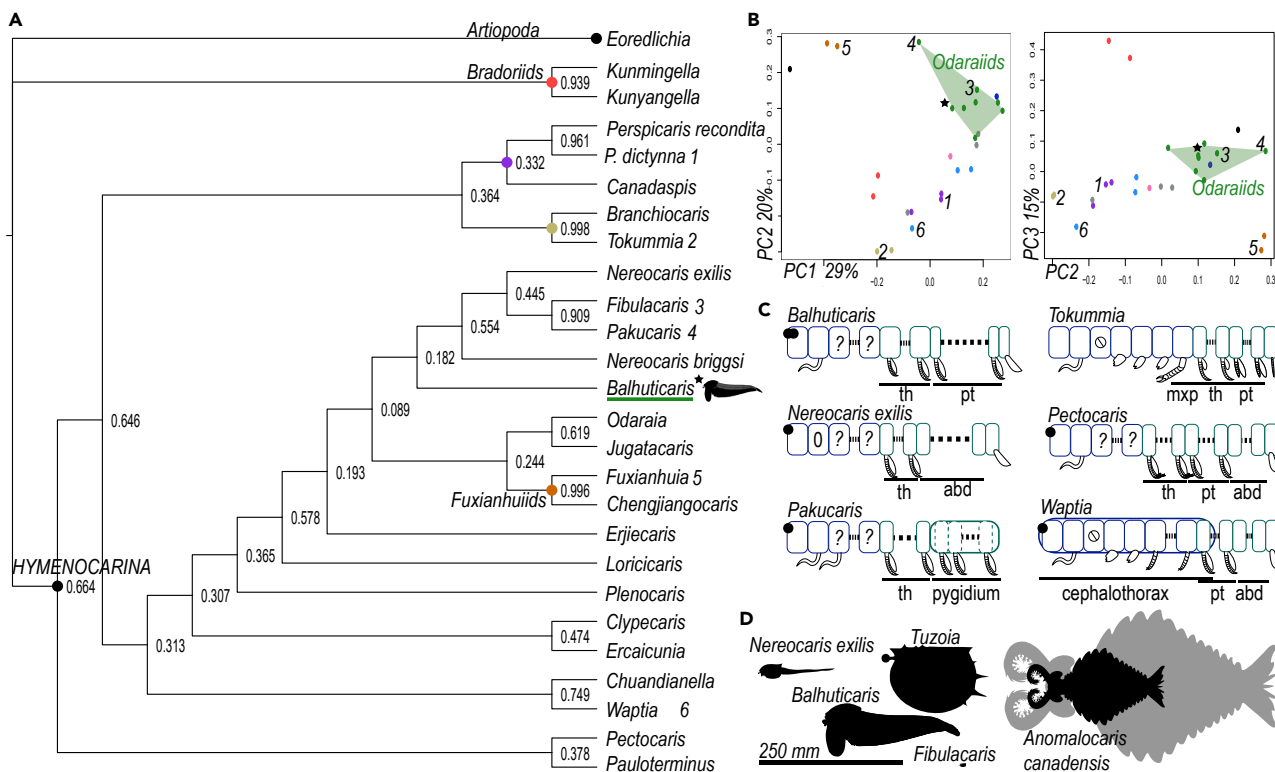


Figure 4. Analyses

(A) Phylogenetic analysis of the hymenocarine-centric dataset.

Consensus tree based on a Bayesian analysis under a Mk model. Numbers represent posterior probabilities.

(B) Morphospace, showcasing coordinates 1–2 (left) and 2–3 (right) of the principal coordinate analysis.

(C) Diagrams of different segmentation patterns across Hymenocarina. Each square represents one segment with its corresponding appendage. Some segments may not bear appendages, or their affinity is unknown. Post-antennular intercalary segments included for comparison, even if not expressed. Dotted lines indicate the presence of an indeterminate number of segments for that tagma. Rounded rectangles indicate segmental fusion.

(D) Size chart comparison, including the biggest hymenocarines and the biggest Burgess Shale arthropod, *Anomalocariscaris*, at 247 mm (ROMIP51214). Claws of 200 mm could hint at the presence of specimens of *Anomalocariscaris* at ca. 600 mm in length (Lerosey-Aubril and Pates, 2018) (gray). Abbreviations: abd, abdomen; mnxp, maxilliped; th, thorax; pt, post-thorax. See also Figure S4.

DISCUSSION

Multisegmentation and tagmatization in early mandibulates

With a total of 110 post-cephalic segments, *Balhuticaris* has the highest number of segments recorded among Cambrian arthropods. Multisegmentation (more than 20 segments, Aria and Caron, 2017) is widely present across Cambrian arthropod groups such as jianfengiids (Aria et al., 2020), marrellomorphs (Rak et al., 2013), and in multiple trilobites. In hymenocarines, multisegmentation is characteristic of “odaraiids” but also protocaridids (Figures S5A and S5B). The range of post-cephalic segment numbers varies widely across “odaraiid” species, with several species having more than 60 segments (e.g., *Nereocaris briggsi*, Legg and Caron, 2014) and some showing a supernumerary number of segments that represent extreme cases of multisegmentation: *Nereocaris exilis* with 90–100 segments (Legg et al., 2012) and *Balhuticaris* with 110 segments. This diversity in the number of post-cephalic segments in “odaraiids” contrasts with the hymenocarine groups Canadaspida, Clypeocaridae, and Waptiidae, in which the number of thoracic segments is highly constrained, close to 10 (in *Waptia*, though, this may depend on the interpretation of the cephalothoracic limbs, Vannier et al., 2018).

The origin of multisegmentation in hymenocarines is a matter of discussion. In extant arthropods, segment addition can occur either simultaneously during embryogenesis, or through a terminal growth zone (Clark et al., 2019) that can continue to add segments sequentially and posteriorly after the embryonic stages (anamorphic development). Helminthomorph millipedes (Fusco, 2005), trilobites (Hughes, 2007), and some crustacean groups (e.g., anostracans, Fryer, 1983, remipedes, Koenemann et al.,

2009) show anamorphic development leading to multisegmentation, but other groups can acquire multisegmentation before ending their embryonic stages (geophilomorphs, Fusco, 2005). The “odaraiid” *Pakucaris* (Izquierdo-López and Caron, 2021) and fuxianhuiids (Fu et al., 2018), potentially closely related to hymenocarines (Aria, 2022), exhibit anamorphic growth, indicating that multisegmentation could have been attained through this type of development. Lifestyles like suspension feeding (Fortey, 2014; Fryer, 2006) and burrowing (in myriapods, Marek et al., 2021) have been suggested to be related to multisegmentation. While suspension feeding was most probably the feeding strategy of many hymenocarines, not all multisegmented hymenocarines were suspension feeders, though (e.g., *Tokummia*, Aria and Caron, 2017). If hymenocarines are early mandibulates, this could suggest that the ancestral mandibulate was multisegmented (Figure S5C) and that the disparate patterns of segmentation in hymenocarines would become more constrained later in crown-pancrustaceans, a pattern that is similarly present through early trilobite evolution (Hughes, 2007). Extreme multisegmentation appears so far to be mostly confined to “odaraiids” and extant myriapods (Figures S5A and S5B). It is not clear why extreme multisegmentation occurs in myriapods or whether is related to any specific lifestyle (Clark et al., 2019), and therefore, the origin of this trait remains unknown.

Balhuticaris also shows a distinct post-cephalic organization, with its thoracic segments much longer than its post-thoracic segments. This pattern is reminiscent of the trilobite protrunk and opisthotrunk (Hughes, 2007) and different pereon-pleon conformations in crustaceans, but also closely resembles a cephalothorax. A cephalothorax is here understood as a unit composed of the head appendages and a series of thoracic appendages that have a distinct morphology, most commonly associated with feeding (maxillipeds). The limbs of this tagma in *Balhuticaris* are not maxilliped-like, and they do not appear highly differentiated, but their frontal reduction in length is still characteristic of the series of maxillipeds in extant crustaceans (e.g., some amphipods (Bellan-Santini, 2015)) and the cephalothorax of the mandibulate hymenocarine *Waptia* (Vannier et al., 2018), which could suggest a certain specialization.

Tagmatization is varied across mandibulates: the trunk of crustaceans is highly diverse, governed by complex interactions in the expression of Hox genes (Martin et al., 2016), while myriapods have a more conservative body plan. Hymenocarines show multiple distinct patterns of tagmatization, including thoracic and post-thoracic differentiation based on the types of endites (e.g., in *Pectocaris*, Jin et al., 2021), the relative length of endopods and exopods (e.g., in *Tokummia*, Aria and Caron, 2017), a limbless abdomen (e.g., in *N. exilis*, Legg et al., 2012), maxillipeds (e.g., in *Tokummia*, Aria and Caron, 2017), or fused thoracic segments in a shield-like structure (pygidium, in *Pakucaris*, Izquierdo-López and Caron, 2021) (Figure 4C). Ancestral character reconstruction using the data available, suggests that if hymenocarines are early mandibulates, their ancestral body plan would possess a multisegmented body that lacked thoracic differentiation but presented an abdomen (Figure S6). Furthermore, the different post-cephalic tagmatizations, coupled with the new segmentation type of *Balhuticaris* and other patterns in fuxianhuiids (e.g., tergo-sternal decoupling), would represent a burst of disparity toward crown-mandibulates and would imply that many Hox-gene pathways that later characterize crown-group crustaceans, such as the hexapod abdomen (Abzhanov and Kaufman, 2000) or post-cephalic limb differentiations (Martin et al., 2016), could have either already existed across early mandibulates or, alternatively, appeared convergently (similarly to the limbless chelicerate opisthosoma, Khadjeh et al., 2012).

Mode of life and functional morphology

The habitus of *Balhuticaris* indicates it was probably a good swimmer, as suggested by its elongated body (Fortey, 2014), lightly sclerotized segments, large paddle-shaped exopods (allowing for metachronal swimming, Briggs and Whittington, 1985), wide caudal rami (allowing it to perform escape reactions), and a small carapace that would reduce weight and drag (Yamada, 2019). Another potential feature related to swimming is the tripartite caudal rami, a feature present only among hymenocarines (Legg and Caron, 2014; Vannier et al., 2018) (Figure S3). In two-segmented uropods, the distal pseudo-segment bends ventrally when the tail repositions itself dorsally after a stroke, reducing drag (Kutschera et al., 2012), and the tripartite condition could perform analogously. Some of these morphological features have also been associated with pelagic lifestyles (Fortey, 2014). The carapace in *Balhuticaris*, as in other hymenocarines (e.g., *Clypecaris*, *Fibulacaris*, Izquierdo-López and Caron, 2019; Yang et al., 2016), extends ventrally beyond the length of the legs, which would impair benthic crawling, reinforcing the notion of a pelagic lifestyle in this species. Pelagic big arthropods, though, have usually a skewed fossil record at the Burgess Shale, represented mostly by moults and a very infrequent recovery of full-bodied specimens (Daley and

Edgecombe, 2014; Vannier et al., 2007, 2009), as well as a wide distribution (Williams et al., 2007), which neither are the case for *Balhuticaris*. For this reason, given the current evidence, we consider that a nekto-benthic lifestyle is most likely, but do not entirely discard a pelagic lifestyle.

To avoid predators, *Balhuticaris* would have relied on its size, swimming ability, and a unique sensory system composed of receptors in the caudal rami and bilobate eyes. The caudal rami have small spines that were probably mechanoreceptors (Strausfeld, 2016), and setae morphologically similar to the simple setae of extant crustaceans, which are generally chemoreceptors or have additional mechanical functions (Garm and Watling, 2013). The eyes are bilobate. Vertically bilobate eyes are present among pelagic crustaceans and are adapted to different light conditions on the upper and lower part of the water column (Land, 1999). Laterally bilobate eyes are present only in some stomatopods (Schiff et al., 2007), in which they provide monocular stereoscopic vision, which improves the analysis of spatial information, size discrimination, and shape resolution (Marshall et al., 1991; Schiff et al., 2007). While this feature is unique so far among Cambrian arthropods, the combination of lateral and median compound eyes in leanchioliids (Aria et al., 2015) could have had a similar function.

The lack of information on the cephalic appendages of *Balhuticaris* makes assessing its feeding mode difficult. Extant arthropods of a similar size, such as giant isopods (Poore and Bruce, 2012), stomatopods (Schram et al., 2013), or caridean lobsters (Wicksten, 2010), are in most cases predators or scavengers. These organisms usually seize or collect prey with chelate or subchelate appendages or (in xiphosurans) grind food with strong gnathobases (Botton, 1984). *Balhuticaris* does not have clear chelate limbs or gnathobases, and this is most probably not the result of preservation bias, as these structures have been preserved in other, smaller hymenocarines (Briggs, 1976, 1978). On the other hand, suspension- and deposit feeding usually depend on filtering structures with dense rows of setae (Kornienko, 2013; Riisgård, 2015). Suspension- and deposit feeders are generally constrained in size, as respiration increases with the cube of body length while filtering structures increase with its square (Humphries, 2007; Riisgård, 2015) so that bigger species need wide filtering structures (e.g., *Aegirocassis*, Van Roy et al., 2015). No such structure is present in *Balhuticaris*, although one is more likely to have been obscured by the carapace in the fossil specimens than big chelate limbs would be.

The homonomous multisegmented body of *Balhuticaris* is reminiscent of that of extant branchiopods, mainly anostracans, and genera like *Branchinecta*, one of the largest anostracans (Fryer, 1966), are potentially good analogs. As *Branchinecta* increases in body size, the relative size of the prey also increases, and endites change from filtering to more stout, spinose structures (Fryer, 1983). The movement of the limbs creates a suction force that is not used to filter organic particles from the water, but to bring prey into a median cage made by the limb's endites, and mechanically transport it to the mouth. The anatomy of *Balhuticaris* suggests a potentially similar feeding strategy: suctioning prey through water currents and transporting it through the ventral groove, although whether this was mechanically aided by the presence of endites at the base of the limbs, is unknown from the fossil material. By capturing bigger, more nutritious prey, size constraints associated with suspension feeding could have been reduced. Similarly-sized extant suspension feeders such as nephropoid lobsters, capture zooplankton through a continuous motion of their setae-bearing mouthparts (Loo et al., 1993) but need to energetically complement this lifestyle with other feeding strategies (e.g., predation, Wahle et al., 2012).

Feeding was probably performed while swimming (as in leptostracans, Riisgård, 2015 or anostracans, Fryer, 1983), or even while swimming in an inverted position (Figure 3F). Inverted swimming appears independently in multiple extant groups (e.g., anostracans and xiphosurans) and has been inferred in other "odaraiid" arthropods (ie., *Odaraia*, *Fibulacaris*, Briggs, 1981; Izquierdo-López and Caron, 2019) (Figure 5). This behavior has been suggested to assist in suspension feeding or to increase stability (Fryer, 2006), but this appears to differ across inverted-swimming species (see Supplemental information). *Balhuticaris* shows some of the traits that are sometimes correlated with this behavior: a carapace that would impair benthic crawling, multisegmentation, and a potential suspension-feeding lifestyle, coupled with previous comparisons to *Branchinecta*, further reinforce the idea that *Balhuticaris* could have swum in this position.

At ca. 245 mm, *Balhuticaris* is the biggest bivalved arthropod known to date, with the closest being *Tuzoia* (170 mm, Vannier et al., 2007) and *N. exilis* (142 mm, Legg et al., 2012) (Figures 4D and 5). *Balhuticaris* is one of the biggest fully preserved animals from the Burgess Shale and the Cambrian (Figures 4D and 5), and one of the few arthropods to reach this size outside of radiodonts (Caron and Moysiuk, 2021; Lerosey-Aubril and

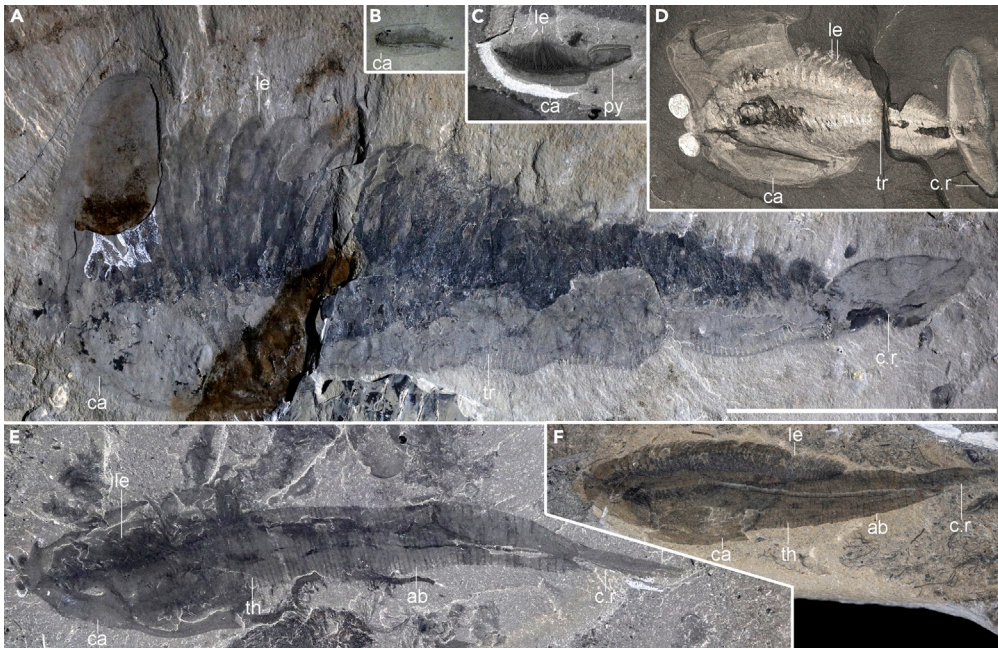


Figure 5. Size comparison of all "odaraids" from the Burgess Shale

Species shown upside-down for comparison, portraying the swimming mode of *Fibulacaris*, *Odaraia*, and potential swimming mode of *Balhuticaris*. All species in lateral view, with the exception of D), in dorsal view.

(A) *Balhuticaris voltae*, this specimen is 171.8 mm in length (ROMIP66238).

(B) *Fibulacaris nereidis*, this specimen is 16.3 mm in length (ROMIP 65380).

(C) *Pakuacaris apatis*, this specimen is 26.6 mm, the biggest specimen known from this species (ROMIP65739).

(D) *Odaraia alata*, this specimen is 56.5 mm in length (ROM 60746).

(E) *Nereocaris exilis*, this specimen is 124.5 mm in length (ROM 61833).

(F) *Nereocaris briggsi*, this specimen is 76.4 mm in length, one of the biggest specimens known from this species (ROM 62164). Abbreviations: ab, abdomen; ca, carapace; c.r., caudal rami; le, legs; py, pygidium; th, thorax; tr, trunk. All species are at the same scale: (A-F) 50 mm.

Pates, 2018) or trilobitomorphs (Holmes et al., 2020; Whittington, 1985). Cambrian bivalved arthropods are generally small, below 100 mm, covered by wide cephalothoracic carapaces. Species such as *N. exilis* (Legg et al., 2012) and *Balhuticaris* have a small carapace, adequate for their active, nekto-benthic lifestyle (see the benthic *N. briggsi* for comparison, Legg and Caron, 2014), trading protection for a lower energetic cost of swimming in upper layers of the water column. Size is known to increase as a response to predation (Vermeij, 2016), and thus, the bigger sizes of *Balhuticaris* and *N. exilis* could have been triggered by this factor. Some of the biggest species at the Burgess Shale were predators (e.g., *Anomalocaris*) and most probably had a similar lifestyle (Briggs, 1975), promoting size increase in prey among other groups. Large suspension feeders can have an important ecological role in translocating matter, subsidizing less productive areas (Hall et al., 2007; Humphries, 2007) and differences in size can allow species to access resources at a different scale, even if their feeding strategy is the same (e.g., suspension feeding) (Kohda et al., 2008). The increasing ecological complexity of the Cambrian has long been recognized based on its planktonic communities (Butterfield, 1997) or the filling of the pelagic zone (Harper et al., 2015; Pates et al., 2021) and species such as *Balhuticaris*, thus, not only exemplify how gigantism in the Cambrian occurred in a wider number of groups than Radiodonta but also exemplify this increasing complexity of the Cambrian ecosystems.

Limitations of the study

The study has a limited number of specimens ($n = 11$). Therefore, the affinity of certain features remains inconclusive (e.g., segmental spines), as well as the delimitation of the morphotypes. Furthermore, the lack of a clear cephalic conformation prevents a definitive mandibulate position, and the monophyly of Hymenocarina remains inconclusive despite the current phylogenetic analyses. Reconstructions of the mode of life are based on functional morphology approaches and extant analogs and could have benefited from

further inferences (e.g., biomechanical modeling). The analysis of patterns of segmentation across euarthropods is mainly focused on bivalved arthropods, but further conclusions would be dependent on a stronger phylogenetic resolution.

STAR★METHODS

Detailed methods are provided in the online version of this paper and include the following:

- KEY RESOURCES TABLE
- RESOURCE AVAILABILITY
 - Lead contact
 - Materials availability
 - Data and code availability
- EXPERIMENTAL MODEL AND SUBJECT DETAILS
- METHOD DETAILS
 - Materials
 - Methods
- QUANTIFICATION AND STATISTICAL ANALYSIS

SUPPLEMENTAL INFORMATION

Supplemental information can be found online at <https://doi.org/10.1016/j.isci.2022.104675>.

ACKNOWLEDGMENTS

We thank five anonymous reviewers for their comments, which helped improving the manuscript. We thank Maryam Akrami and Peter Fenton for their assistance in the Royal Ontario Museum paleobiology collection, as well as Hugo Salais for the reconstructions and Sara Scharf for editorial suggestions. A.I.-L. thanks Cédric Aria, Joe Moysiuk, Karma Nanglu, and Danielle de Carle for their feedback. We thank Parks Canada and Todd Keith for facilitating fieldwork activities. Fossils for this study were collected by Royal Ontario Museum field parties under several Parks Canada Research and Collections permits to J.-B.C. (YNP2012-2054, KOONIP 2014–16317; YNP-2016-21639; KOONP-2018-28179). This research was undertaken as part of a PhD thesis (A.I.-L.), supported by doctoral fellowships from the University of Toronto Department of Ecology and Evolutionary Biology, funding from 'la Caixa' Foundation (ID100010434) under agreement (LCF/BQ/AA18/11680039) to A.I.-L. and a Natural Sciences and Engineering Research Council of Canada of Canada Discovery Grant (#341944) to J.-B.C. This is Burgess Shale Project number 92.

AUTHOR CONTRIBUTIONS

A.I.-L. and J.-B.C. analyzed the material. A.I.-L. wrote an initial version of the manuscript and both authors contributed to the final manuscript. J.-B.C. prepared and photographed the material. A.I.-L. compiled bibliography and performed analyses. A.I.-L. and J.-B.C. created the figures.

DECLARATION OF INTERESTS

The authors declare no competing interests.

Received: February 10, 2022

Revised: April 13, 2022

Accepted: June 22, 2022

Published: July 15, 2022

REFERENCES

- Abzhanov, A., and Kaufman, T.C. (2000). Crustacean (malacostracan) Hox genes and the evolution of the arthropod trunk. *Development* 127, 2239–2249. <https://doi.org/10.1242/dev.127.11.2239>.
- Aria, C. (2022). The origin and early evolution of arthropods. *Biol. Rev. Camb. Philos. Soc.* <https://doi.org/10.31233/osf.io/4zmev>.
- Aria, C. (2020). Macroevolutionary patterns of body plan canalization in euarthropods. *Paleobiology* 46, 569–593. <https://doi.org/10.1017/pab.2020.36>.
- Aria, C., and Caron, J.B. (2017). Burgess Shale fossils illustrate the origin of the mandibulate body plan. *Nature* 545, 89–92. <https://doi.org/10.1038/nature22080>.
- Aria, C., and Caron, J.B. (2015). Cephalic and limb anatomy of a new isoxyid from the Burgess Shale and the role of “stem bivalved arthropods” in the disparity of the frontalmost appendage. *PLoS One* 10, e0124979. <https://doi.org/10.1371/journal.pone.0124979>.
- Aria, C., Caron, J.B., and Gaines, R. (2015). A large new leancoilloid from the Burgess Shale and the

- influence of inapplicable states on stem arthropod phylogeny. *Palaeontology* 58, 629–660. <https://doi.org/10.1111/pala.12161>.
- Aria, C., Zhao, F., Zeng, H., Guo, J., and Zhu, M. (2020). Fossils from South China redefine the ancestral euarthropod body plan. *BMC Evol. Biol.* 20, 4. <https://doi.org/10.1186/s12862-019-1560-7>.
- Aria, C., Zhao, F., and Zhu, M. (2021). Fuxianhuidi are mandibulates and share affinities with total-group Myriapoda. *J. Geol. Soc. London.* 178, jgs2020–246. <https://doi.org/10.1144/jgs2020-246>.
- Bellán-Santini, D. (2015). Order Amphipoda latreille, 1816. In *Treatise on Zoology-Anatomy, Taxonomy, Biology. The Crustacea, Volume 5*, J.C. von Vaupel Klein, M. Charmantier-Daures, and F.R. Schram, eds. (Koninklijke Brill NV), pp. 93–248.
- Botton, M.L. (1984). Diet and food preferences of the adult horseshoe crab *Limulus polyphemus* in Delaware Bay, New Jersey, USA. *Mar. Biol.* 81, 199–207. <https://doi.org/10.1007/BF00393118>.
- Briggs, D.E.G. (1981). The arthropod *Odaraia alata* Walcott, Middle Cambrian, Burgess Shale, British Columbia. *Philos. Trans. R. Soc. Lond. B Biol. Sci.* 291, 541–582. <https://doi.org/10.1098/rstb.1981.0007>.
- Briggs, D.E.G. (1978). The morphology, mode of life, and affinities of *Canadaspis perfecta* (Crustacea: Phyllocarida), middle Cambrian, Burgess Shale, British Columbia. *Philos. Trans. R. Soc. Lond. Ser. B Biol. Sci.* 281, 439–487. <https://doi.org/10.1098/rstb.1978.0005>.
- Briggs, D.E.G. (1976). In *The Arthropod Branchiocaris N. gen., Middle Cambrian, Burgess Shale, British Columbia, 264 The Arthropod Branchiocaris N. gen., Middle Cambrian, Burgess Shale, British Columbia* (Geological Survey of Canada, Energy, Mines and Resources Canada), pp. 1–29.
- Briggs, D.E.G. (1975). *Anomalocaris*, the largest known Cambrian arthropod. *Palaeontology* 22, 631–664.
- Briggs, D.E.G., and Whittington, H.B. (1985). Modes of life of arthropods from the Burgess Shale, British Columbia. *Trans. R. Soc. Edinburgh* 76, 149–160. <https://doi.org/10.1017/S0263593300010415>.
- Butterfield, N.J. (1997). Plankton ecology and the Proterozoic-Phanerozoic transition. *Paleobiology* 23, 247–262. <https://doi.org/10.1017/S009483730001681X>.
- Caine, E.A. (1974). Comparative functional morphology of feeding in three species of caprellids (Crustacea, Amphipoda) from the northwestern Florida gulf coast. *J. Exp. Mar. Bio. Ecol.* 15, 81–96. [https://doi.org/10.1016/0022-0981\(74\)90065-3](https://doi.org/10.1016/0022-0981(74)90065-3).
- Caron, J.-B., and Moysiuk, J. (2021). A giant nektobenthic radiodont from the Burgess Shale and the significance of hurdiid carapace diversity. *R. Soc. Open Sci.* 8, 210664. <https://doi.org/10.1098/rsos.210664>.
- Caron, J.B., Gaines, R.R., Aria, C., Mángano, M.G., and Streng, M. (2014). A new phyllopod bed-like assemblage from the Burgess Shale of the Canadian Rockies. *Nat. Commun.* 5, 3210. <https://doi.org/10.1038/ncomms4210>.
- Caron, J.B., and Vannier, J. (2016). Waptia and the diversification of brood care in early arthropods. *Curr. Biol.* 26, 69–74. <https://doi.org/10.1016/j.cub.2015.11.006>.
- Clark, E., Peel, A.D., and Akam, M. (2019). Arthropod segmentation. *Development* 146, dev170480. <https://doi.org/10.1242/dev.170480>.
- Core Team, R. (2021). R: A Language and Environment for Statistical Computing. (R Foundation for Statistical Computing, Vienna, Austria).
- Daley, A.C., and Edgecombe, G.D. (2014). Morphology of *Anomalocaris canadensis* from the Burgess Shale. *J. Paleontol.* 88, 68–91. <https://doi.org/10.1666/13-067>.
- Fortey, R. (2014). The palaeoecology of trilobites. *J. Zool.* 292, 250–259. <https://doi.org/10.1111/jzo.12108>.
- Fryer, G. (2006). The brine shrimp's tale: a topsy turvy evolutionary fable. *Biol. J. Linn. Soc.* 88, 377–382. <https://doi.org/10.1111/j.1095-8312.2006.00623.x>.
- Fryer, G. (1983). Functional ontogenetic changes in *Branchinecta ferox* (Milne-Edwards) (Crustacea: Anostraca). *Philos. Trans. R. Soc. Lond. B Biol. Sci.* 303, 229–343. <https://doi.org/10.1098/rstb.1983.0097>.
- Fryer, G. (1966). *Branchinecta gigas* Lynch, a non-filter-feeding raptatory anostracan, with notes on the feeding habits of certain other anostracans. *Proc. Linn. Soc. London* 177, 19–34. <https://doi.org/10.1111/j.1095-8312.1966.tb00948.x>.
- Fu, D., Ortega-Hernández, J., Daley, A.C., Zhang, X., and Shu, D. (2018). Anamorphic development and extended parental care in a 520 million-year-old stem-group euarthropod from China. *BMC Evol. Biol.* 18, 147. <https://doi.org/10.1186/s12862-018-1262-6>.
- Fusco, G. (2005). Trunk segment numbers and sequential segmentation in myriapods. *Evol. Dev.* 7, 608–617. <https://doi.org/10.1111/j.1525-142X.2005.05064.x>.
- Garm, A., and Watling, L. (2013). The crustacean integument: setae, setules, and other ornamentation. In *Functional Morphology and Diversity (Natural History of the Crustacea)*, L. Watling and M. Thiel, eds. (Oxford University Press), pp. 167–198.
- Hall, R.O., Koch, B.J., Marshall, M.C., Taylor, B.W., and Tronstad, L.M. (2007). How body size mediates the role of animals in nutrient cycling in aquatic ecosystems. In *Body Size and the Structure and Function of Aquatic Ecosystems*, A. Hildrew, D. Raffaelli, and R. Edmonds-Brown, eds. (Cambridge University Press), pp. 286–305.
- Harper, D.A.T., Zhan, R.B., and Jin, J. (2015). The Great Ordovician Biodiversification Event: reviewing two decades of research on diversity's big bang illustrated by mainly brachiopod data. *Palaeoworld* 24, 75–85. <https://doi.org/10.1016/j.palwor.2015.03.003>.
- Haug, J.T., Caron, J.B., and Haug, C. (2013). Demecology in the Cambrian: synchronized molting in arthropods from the Burgess Shale. *BMC Biol.* 11, 64. <https://doi.org/10.1186/1741-7007-11-64>.
- Hegna, T.A., Legg, D.A., Møller, O.S., Roy, P.V., and Lerosey-Aubril, R. (2013). The correct authorship of the taxon name “Arthropoda”. *Arthropod Syst. Phylogeny* 71, 71–74.
- Holmes, J.D., Paterson, J.R., and García-Bellido, D.C. (2020). The trilobite *Redlichia* from the lower Cambrian Emu Bay Shale Konservat-lagerstätte of South Australia: systematics, ontogeny and soft-part anatomy. *J. Syst. Palaeontol.* 18, 295–334. <https://doi.org/10.1080/14772019.2019.1605411>.
- Xian-Guang, H. (1999). New rare bivalved arthropods from the lower Cambrian Chengjiang fauna, Yunnan, China. *J. Paleontol.* 73, 102–116. <https://doi.org/10.1017/s002233600002758x>.
- Xian-Guang, H., Siveter, D.J., Aldridge, R.J., and Siveter, D.J. (2009). A new arthropod in chain-like associations from the chengjiang lagerstätte (Lower Cambrian), Yunnan, China. *Palaeontology* 52, 951–961. <https://doi.org/10.1111/j.1475-4983.2009.00889.x>.
- Hughes, N.C. (2007). The evolution of trilobite body patterning. *Annu. Rev. Earth Planet Sci.* 35, 401–434. <https://doi.org/10.1146/annurev.earth.35.031306.140258>.
- Humphries, T. (2007). Body size and suspension feeding. In *Body Size and the Structure and Function of Aquatic Ecosystems*, A. Hildrew, D. Raffaelli, and R. Edmonds-Brown, eds. (Cambridge University Press), pp. 16–32.
- Izquierdo-López, A., and Caron, J.B. (2021). A Burgess Shale mandibulate arthropod with a pygidium: a case of convergent evolution. *Pap. Palaeontol.* 7, 1877–1894. <https://doi.org/10.1002/spp2.1366>.
- Izquierdo-López, A., and Caron, J.B. (2019). A possible case of inverted lifestyle in a new bivalved arthropod from the Burgess Shale. *R. Soc. Open Sci.* 6, 191350. <https://doi.org/10.1098/rsos.191350>.
- Jin, C., Mai, H., Chen, H., Liu, Y.U., Hou, X.-G., Wen, R., and Zhai, D. (2021). A new species of the Cambrian bivalved euarthropod *Pectocaris* with axially differentiated enditic armatures. *Pap. Palaeontol.* 7, 1781–1792. <https://doi.org/10.1002/spp2.1362>.
- Khadjeh, S., Turetzek, N., Pechmann, M., Schwager, E.E., Wimmer, E.A., Damen, W.G.M., and Prpic, N.M. (2012). Divergent role of the Hox gene *Antennapedia* in spiders is responsible for the convergent evolution of abdominal limb repression. *Proc. Natl. Acad. Sci. USA* 109, 4921–4926. <https://doi.org/10.1073/pnas.1116421109>.
- Koenemann, S., Olesen, J., Alwes, F., Iliffe, T.M., Hoenemann, M., Ungerer, P., Wolff, C., and Scholtz, G. (2009). The post-embryonic development of Remipedia (Crustacea) — additional results and new insights. *Dev. Genes Evol.* 219, 131–145. <https://doi.org/10.1007/s00427-009-0273-0>.
- Kohda, M., Shibata, J.Y., Awata, S., Gomagano, D., Takeyama, T., Hori, M., and Heg, D. (2008).

- Niche differentiation depends on body size in a cichlid fish: a model system of a community structured according to size regularities. *J. Anim. Ecol.* 77, 859–868. <https://doi.org/10.1111/j.1365-2656.2008.01414.x>.
- Kornienko, E.S. (2013). Burrowing shrimp of the infraorders Gebiidea and Axiidea (Crustacea: Decapoda). *Russ. J. Mar. Biol.* 39, 1–14. <https://doi.org/10.1134/S10663074013010033>.
- Kutschera, V., Maas, A., and Waloszek, D. (2012). Uropods of Eumalacostraca (Crustacea s.l.: Malacostraca) and their phylogenetic significance. *Arthropod Syst. Phylogeny* 70, 181–206.
- Land, M.F. (1999). Compound eye structure: matching eye to environment. In *Adaptive Mechanisms in the Ecology of Vision*, S.N. Archer, M.B.A. Djamgoz, E.R. Loew, J.C. Partridge, and S. Vallerga, eds. (Springer Science+Business Media), pp. 51–71. https://doi.org/10.1007/978-94-017-0619-3_3.
- Legg, D.A., and Caron, J.B. (2014). New middle Cambrian bivalved arthropods from the Burgess Shale (British Columbia, Canada). *Palaeontology* 57, 691–711. <https://doi.org/10.1111/pala.12081>.
- Legg, D.A., Sutton, M.D., Edgecombe, G.D., and Caron, J.B. (2012). Cambrian bivalved arthropod reveals origin of arthropodization. *Proc. R. Soc. B Biol. Sci.* 279, 4699–4704. <https://doi.org/10.1098/rspb.2012.1958>.
- Lerosey-Aubril, R., and Pates, S. (2018). New suspension-feeding radiodont suggests evolution of microplanktivory in Cambrian macronekton. *Nat. Commun.* 9, 3774. <https://doi.org/10.1038/s41467-018-06229-7>.
- Loo, L.O., Pihl Baden, S., and Ulmestrand, M. (1993). Suspension feeding in adult *Nephrops norvegicus* (L.) and *Homarus gammarus* (L.) (Decapoda). *Netherlands J. Sea Res.* 31, 291–297. [https://doi.org/10.1016/0077-7579\(93\)90029-R](https://doi.org/10.1016/0077-7579(93)90029-R).
- Macneil, C., Dick, J.T.A., and Elwood, R.W. (1997). The trophic ecology of freshwater *Gammarus* spp. (crustacea: Amphipoda): Problems and perspectives concerning the functional feeding group concept. *Biol. Rev.* 72, 349–364. <https://doi.org/10.1111/j.1469-185X.1997.tb00017.x>.
- Maddison, W., and Maddison, D. (2009). *Mesquite: A Modular System for Evolutionary Analysis V3.4* (GNU Software).
- Maechler, M., Rousseeuw, P., Struyf, A., Hubert, M., and Hornik, K. (2019). *cluster: Cluster Analysis Basics and Extensions* (R package version 2.1.2).
- Marek, P.E., Buzatto, B.A., Shear, W.A., Means, J.C., Black, D.G., Harvey, M.S., and Rodriguez, J. (2021). The first true millipede — 1306 legs long. *Sci. Rep.* 11, 23126. <https://doi.org/10.1038/s41598-021-02447-0>.
- Marshall, N.J., Land, M.F., King, C.A., and Cronin, T.W. (1991). The compound eyes of mantis shrimps (Crustacea, Hoplocarida, Stomatopoda). I. Compound eye structure: the detection of polarized light. *Philos. Trans. R. Soc. London B* 334, 33–56.
- Martin, A., Serano, J.M., Jarvis, E., Bruce, H.S., Wang, J., Ray, S., Barker, C.A., O'Connell, L., O'Connell, L.C., and Patel, N.H. (2016). CRISPR/Cas9 mutagenesis reveals versatile roles of Hox genes in crustacean limb specification and evolution. *Curr. Biol.* 26, 14–26. <https://doi.org/10.1016/j.cub.2015.11.021>.
- Mayers, B., Aria, C., and Caron, J.B. (2018). Three new naraoiid species from the Burgess Shale, with a morphometric and phylogenetic reinvestigation of Naraoiidae. *Palaeontology* 62, 19–50. <https://doi.org/10.1111/pala.12383>.
- Meyer, D., Zeileis, A., and Hornik, K. (2020). *vcd: Visualizing Categorical Data* (R package version 1.4-9).
- Miller, S.A. (1889). *North American Geology and Palaeontology for the Use of Amateurs, Students and Scientists* (Western Methodist Book Concern).
- Murdoch, D., and Adler, D. (2021). *rgl: 3D Visualization Using OpenGL* (R package version 0.108.3).
- Nanglu, K., Caron, J.B., and Gaines, R.R. (2020). The Burgess Shale paleocommunity with new insights from Marble Canyon, British Columbia. *Paleobiology* 46, 58–81. <https://doi.org/10.1017/pab.2019.42>.
- Oksanen, J., Guillaume Blanchet, F., Friendly, M., Kindt, R., Legendre, P., McGinn, D., and Peter, R. (2020). *vegan: Community Ecology Package* (R package version 2.5-7).
- Olesen, J. (2013). The crustacean carapace: morphology, function, development, and phylogenetic history. In *Functional Morphology and Diversity* (Natural History of the Crustacea), L. Watling and M. Thiel, eds. (Oxford University Press), pp. 103–139.
- Orlov, Y.A. (1960). *Osnovy Paleontologii. In Arthropoda, Trilobitomorpha and Crustacea* (Nedra).
- Pates, S., Daley, A.C., Legg, D.A., and Rahman, I.A. (2021). Vertically migrating *Isoxys* and the early Cambrian biological pump. *Proc. R. Soc. B Biol. Sci.* 288, 20210464. <https://doi.org/10.1098/rspb.2021.0464>.
- Poore, G.C.B., and Bruce, N.L. (2012). Global diversity of marine isopods (except Asellota and Crustacean Symbionts). *PLoS One* 7. <https://doi.org/10.1371/journal.pone.0043529>.
- Rak, Š., Ortega-Hernández, J., and Legg, D.A. (2013). A revision of the Late Ordovician marrellomorph arthropod *Furca bohemica* from Czech Republic. *Acta Palaeontol. Pol.* 58, 615–628. <https://doi.org/10.4202/app.2011.0038>.
- Rambaut, A., Drummond, A.J., Xie, D., Baele, G., and Suchard, M.A. (2018). Posterior summarization in Bayesian phylogenetics using tracer 1.7. *Syst. Biol.* 67, 901–904. <https://doi.org/10.1093/sysbio/syy032>.
- Revell, L.J. (2012). *phytools: an R package for phylogenetic comparative biology (and other things)*. *Methods Ecol. Evol.* 3, 217–223. <https://doi.org/10.1111/j.2041-210X.2011.00169.x>.
- Riisgård, H.U. (2015). Filter-feeding mechanisms in crustaceans. In *Lifestyles and Feeding Biology. The Natural History of the Crustacea 2*, M. Thiel and L. Watling, eds. (Oxford University Press), pp. 418–463.
- Ronquist, F., Teslenko, M., Van Der Mark, P., Ayres, D.L., Darling, A., Höhna, S., Larget, B., Liu, L., Suchard, M.A., and Huelsenbeck, J.P. (2012). MrBayes 3.2: efficient Bayesian phylogenetic inference and model choice across a large model space. *Syst. Biol.* 61, 539–542. <https://doi.org/10.1093/sysbio/sys029>.
- Schiff, H., Dore, B., and Boido, M. (2007). Morphology of adaptation and morphogenesis in stomatopod eyes. *Ital. J. Zool.* 74, 123–134. <https://doi.org/10.1080/11250000701245866>.
- Schram, F.R., Ah Yong, S.T., Patek, S.N., Green, P.A., Rosario, M.V., Bok, M.J., Cronin, T.W., Mead Vetter, K.S., Caldwell, R.L., Scholtz, G., et al. (2013). Subclass hoplocarida Calman, 1904: order stomatopoda Latreille, 1817. In *Treatise on Zoology-Anatomy, Taxonomy, Biology. The Crustacea, Volume 4*, J.C. von Vaupel Klein, M. Charmantier-Daures, and F.R. Schram, eds. (Brill), pp. 179–356. Part A.
- Snodgrass, R.E. (1938). *Evolution of the Annelida, Onychophora and Arthropoda*. *Smithson. Misc. Collect.* 97.
- Strausfeld, N.J. (2016). *Waptia* revisited: intimations of behaviors. *Arthropod Struct. Dev.* 45, 173–184. <https://doi.org/10.1016/j.asd.2015.09.001>.
- Van Roy, P., Daley, A.C., and Briggs, D.E.G. (2015). Anomalocaridid trunk limb homology revealed by a giant filter-feeder with paired flaps. *Nature* 522, 77–80. <https://doi.org/10.1038/nature14256>.
- Vannier, J., Aria, C., Taylor, R.S., and Caron, J.B. (2018). *Waptia fieldensis* Walcott, a mandibulate arthropod from the middle Cambrian Burgess Shale. *R. Soc. Open Sci.* 5, 172206. <https://doi.org/10.1098/rsos.172206>.
- Vannier, J., Caron, J.B., Yuan, J.L., Briggs, D.E.G., Collins, D., Zhao, Y.L., and Zhu, M.Y. (2007). *Tuzoia*: morphology and lifestyle of a large bivalved arthropod of the Cambrian seas. *J. Paleontol.* 81, 445–471. <https://doi.org/10.1666/05070.1>.
- Vannier, J., García-Bellido, D., Hu, S.X., and Chen, A.L. (2009). Arthropod visual predators in the early pelagic ecosystem: evidence from the Burgess Shale and Chengjiang biotas. *Proc. R. Soc. B Biol. Sci.* 276, 2567–2574. <https://doi.org/10.1098/rspb.2009.0361>.
- Vermeij, G.J. (2016). Gigantism and its implications for the history of life. *PLoS One* 11, e0146092. <https://doi.org/10.1371/journal.pone.0146092>.
- Wahle, R.A., Tshudy, D., Stanley Cobb, J., Factor, J., and Jaini, M. (2012). *Infraorder Astacidea Latreille, 1802 p.p.: the marine clawed lobsters*. In *The Crustacea Revised and Updated from the Traité de Zoologie Volume 9 Part B*, F.R. Schram and J.C. von Vaupel Klein, eds. (Brill), pp. 3–108.
- Walcott, C.D. (1912). *Cambrian geology and paleontology II: middle Cambrian branchiopoda*.

malacostraca, trilobita and Merostomata. *Smithson. Misc. Collect.* 57, 145–228.

Whittington, H.B. (1985). *Tegopelte gigas*, a second soft-bodied trilobite from the Burgess Shale, middle Cambrian, British Columbia. *J. Paleontol.* 59, 1251–1274.

Wicksten, M.K. (2010). Infraorder Caridea Dana, 1852. In *The Crustacea, Revised and Updated from the Traité de Zoologie. V9 Part A*, F.R. Schram and V. Klein, eds. (Brill), pp. 165–214.

Williams, M., Siveter, D.J., Popov, L.E., and Vannier, J.M.C. (2007). Biogeography and affinities of the bradoriid arthropods:

cosmopolitan microbenthos of the Cambrian seas. *Palaeogeogr. Palaeoclimatol. Palaeoecol.* 248, 202–232. <https://doi.org/10.1016/j.palaeo.2006.12.004>.

Yamada, S. (2019). Ultrastructure and cuticle formation of the carapace in the myodocopan ostracod exemplified by *Euphilomedes japonica* (Crustacea: Ostracoda). *J. Morphol.* 280, 809–826. <https://doi.org/10.1002/jmor.20985>.

Yang, J., Ortega-Hernández, J., Lan, T., Hou, J.B., and Zhang, X.G. (2016). A predatory bivalved euarthropod from the Cambrian (stage 3) Xiaoshiba lagerstätte, South China.

Sci. Rep. 6, 27709. <https://doi.org/10.1038/srep27709>.

Zeng, H., Zhao, F.-C., Yin, Z.-J., and Zhu, M.-Y. (2020). A new early Cambrian bivalved euarthropod from Yunnan, China and general interspecific morphological and size variations in Cambrian hymenocarines. *Palaeoworld* 30, 387–397. <https://doi.org/10.1016/j.palwor.2020.09.002>.

Zhai, D., Ortega-Hernández, J., Wolfe, J.M., Hou, X.-G., Cao, C., and Liu, Y. (2019). Three-dimensionally preserved appendages in an early Cambrian stem-group pancrustacean. *Curr. Biol.* 29, 171–177.e1. <https://doi.org/10.1016/j.cub.2018.11.060>.

STAR★METHODS

KEY RESOURCES TABLE

REAGENT OR RESOURCE	SOURCE	IDENTIFIER
Biological samples		
Specimens of <i>Balhuticaris voltae</i>	Royal Ontario Museum	See Table S4 for reference
Software and algorithms		
Adobe Illustrator 2020	Adobe Systems	
RStudio, R	Core Team (2021)	V.4.1.0
Mesquite	Maddison and Maddison (2009)	V3.4
Mr Bayes	Ronquist et al. (2012)	V3.2
Tracer	Rambaut et al. (2018)	V1.7.1
R packages: <i>phytools</i> , <i>cluster</i> , <i>vegan</i> , <i>vcd</i> , <i>rgl</i>	Maechler et al. (2019) ; Meyer et al. (2020) ; Murdoch and Adler (2021) ; Oksanen et al. (2020) ; Revell (2012)	V0.7–90; V2.1.2; V2.5–7; V1.4–8; V0.106.8

RESOURCE AVAILABILITY

Lead contact

Requests for further information should be directed to and will be fulfilled by the Lead Contact, Alejandro Izquierdo López (ai.lopez@mail.utoronto.ca).

Materials availability

This study did not generate new unique materials.

Data and code availability

- Codes necessary for the hymenocarine phylogenetic analysis ([Data Files 1 and 2](#), related to [Figure 4](#)) and euarthropod analysis ([Data Files 3 and 4](#), related to [Figure S4](#)), and data for the segmentation analysis ([Data File 5](#), related to [Figures S5 and S6](#)) are available for download as [Data S1](#).
- Code necessary for the morphospace (related to [Figure 4](#)) and segmentation analysis (related to [Figures S5 and S6](#)) are included as [Data File 6](#) in [Data S1](#).
- Supplementary figures and character list are available for download as [Document S1](#).

EXPERIMENTAL MODEL AND SUBJECT DETAILS

The experimental model and subject of this study only includes fossil specimens.

METHOD DETAILS

Materials

A total of eleven specimens ([Table S4](#)) were collected *in situ* from the upper part of the thick Burgess Shale formation: three specimens were obtained from the Marble Canyon locality ([Caron et al., 2014](#)) (Kootenay National Park, British Columbia, Canada) in the 2012 and 2016 expeditions, one specimen previously referred as “New Dinocariid B” (ROMIP66236, [Nanglu et al., 2020](#)). A total of eight additional specimens were obtained from an adjacent outcrop, stratigraphically equivalent, during the 2018 expedition ([Mayers et al., 2018](#)). Preparation revealed an additional individual in one specimen (ROMIP66243), both partially preserved. All specimens were deposited at the Royal Ontario Museum Invertebrate Paleontology Collection (ROMIP). The new nomenclatural act has been registered in ZooBank: LSID: urn:lsid:zoobank.org:pub:D5D074C5-88A1-4994-8D4E-F73283AEDFE3.

Methods

Multiple specimens were prepared using an air scribe, removing the matrix covering anatomical features. In order to access cephalic appendages, preparation was also used to remove parts of the carapace covering

the cephalic region of one specimen (ROMIP66238). All specimens were directly photographed under direct or cross-polarized conditions, both in wet and dry conditions.

QUANTIFICATION AND STATISTICAL ANALYSIS

The first analysis is based on a new dataset focused on hymenocarines (hymenocarine-centric) with a total of 26 taxa (21 hymenocarines) and 114 characters, binary or multistate, unordered and unweighted. A Bayesian phylogenetic analysis was performed with MrBayes 3.2.6, using a Markov k (Mk) model with rate variation under a gamma distribution, using 4 runs and 4 chains for 20 million generations, sampling every 1,000 generations and a 25% burn-in. Convergence of the runs was analyzed with Tracer V.1.7.1. This analysis aimed to test local synapomorphies within the hymenocarines and increase support values. The second phylogenetic analysis was a Bayesian analysis based on a previous dataset (Aria et al., 2020), which includes a broad sample of taxa across Euarthropoda (see [Supplemental information](#)). To this dataset, we added additional taxa and characters based on an extended dataset (Aria et al., 2021), as well as a comprehensive sample of hymenocarines and important characters extracted from the first phylogenetic analysis (See [Supplemental information](#)).

Using the hymenocarine-centric dataset, a morphospace analysis was performed. This analysis is a principal coordinate analysis on a dissimilarity matrix with the metric *gower* of the *cluster* R package, which allows for the presence of non-applicable states (Maechler et al., 2019). We also obtained the total number of segments for each terminal of the second phylogenetic dataset from the literature (see [Supplemental information](#)). Using this data, when applicable, we performed ancestral trait reconstruction with ML using the function *contMap* of the R package *phytools* and plotted it onto the phylogeny. Similarly, we coded the presence of the abdomen for the mandibulates in the euarthropod dataset and traced it with ML in *Mesquite*.